

High transverse momentum suppression and surface effects in Cu+Cu and Au+Au collisions within the PQM model

Constantin Loizides^{1,2}

¹ Massachusetts Institute of Technology, 77 Massachusetts Avenue, Cambridge, MA 02139, USA

² Email: loizides@mit.edu

Received: August 7, 2018 / Revised version: August 7, 2018

Abstract. We study parton suppression effects in heavy-ion collisions within the Parton Quenching Model (PQM). After a brief summary of the main features of the model, we present comparisons of calculations for the nuclear modification and the away-side suppression factor to data in Au+Au and Cu+Cu collisions at $\sqrt{s_{NN}} = 200$ GeV. We discuss properties of light hadron probes and their sensitivity to the medium density within the PQM Monte Carlo framework.

1 Introduction

One of the very early and very exciting findings from the experiments running at the Relativistic Heavy Ion Collider (RHIC) was the observation of apparent jet suppression. At the top RHIC energy, $\sqrt{s_{NN}} = 200$ GeV, the mid-rapidity yield of high transverse momentum leading particles in Au+Au collisions is about a factor of five lower than expected from the measurements in p+p collisions at the same energy [1, 2]. Similarly, jet-like correlations on the azimuthally-opposite ('away') side of a high- p_t trigger particle are suppressed by a factor of four to five, while the near-side correlation strength is almost unchanged [3]. The observed suppression persists also at lower center-of-mass energies [4], as well as in Cu+Cu collisions at 62.4 and 200 GeV [5]. The absence of these effects in d+Au collisions at $\sqrt{s_{NN}} = 200$ GeV [6] strongly supports the picture of partonic energy loss, where energetic partons, produced in initial hard scattering processes, lose energy as a consequence of the final-state interaction with the dense partonic matter created in nucleus-nucleus collisions. The dominant contribution to the energy loss is believed to originate from medium-induced gluon radiation (see Ref. [7] and references therein). Recent calculations point out, however, that the collisional contribution to the energy loss might not be negligible [8]. Still, strong interest in these probes arises mainly from the fact that modification of their properties due to interaction with the medium provides access to fundamental properties of the created matter, such as its density and nature [9].

A quite simple model that includes final-state gluon radiation is the Parton Quenching Model (PQM) [10]. It combines the pQCD BDMPS-Z-SW framework for the probabilistic calculation of parton energy loss in extended partonic matter of given size and density [11] with a realistic description of the collision overlap geometry in a static medium. High-energy partons (and parton pairs)

are treated on an event-by-event basis using Monte Carlo techniques. The model has one single free parameter that sets the scale of the medium transport coefficient \hat{q} , the average transverse momentum squared transferred to the hard parton per unit path length, and, thus, the scale of the energy loss.

In these proceedings, we will, after a short introduction to the PQM model, compare the suppression phenomena introduced above to the calculations obtained with PQM. In particular, we will discuss to what extent light hadronic probes are sensitive to the dense matter formed at RHIC.

2 The PQM model

The Monte Carlo calculation of the unquenched and quenched transverse momentum spectra in PQM consists of four main steps: 1) Determination of a parton type and its transverse momentum according to PYTHIA (LO) parton distribution functions. 2) Determination of its parton-production point in the transverse plane according to the nuclear density profile (Glauber) and evaluation of path length and transport coefficient seen by the produced parton using two line integrals weighted with ρ_{coll} . 3) Calculation of the energy loss using constrained quenching weights to extrapolate from the eikonal approach used in the BDMPS-SW framework to finite parton energies. Two types of constraints are constructed to estimate the systematic uncertainty of the approach: In the reweighted case the energy-loss distribution is simply normalized within the kinematically allowed regime, whereas in the non-reweighted case the fraction of the distribution larger than the energy of the parton contributes to the probability of maximum energy loss. 4) Finally, independent fragmentation is applied to the quenched and original parton. Back-to-back parton pairs initially consist of a pair of partons

with the same p_t at the same production point, but with opposite-side emission angle.

Currently, the model is restricted to mid-rapidity, and, for simplicity, we ignore initial-state effects. The single parameter of the model (k) is fixed to set the scale of the energy loss by fitting to data from 0–10% central Au+Au collisions at $\sqrt{s_{NN}} = 200$ GeV. Once the scale is fixed we implicitly vary the medium density by its dependence on the centrality as given by Glauber.

Details on the quenching procedure and its application to high- p_t data can be found in Ref. [10].

3 Suppression of leading particles

Suppression of leading particles is usually quantified via the nuclear modification factor,

$$R_{AA}(p_t, \eta) \equiv \frac{1}{\langle N_{\text{coll}} \rangle} \times \frac{d^2 N_{AA}/dp_t d\eta}{d^2 N_{pp}/dp_t d\eta}, \quad (1)$$

the ratio of the yield of light hadrons in nucleus–nucleus over proton–proton yield scaled by the number of binary collisions in a given centrality class. The ratio is normalized so that, if no final-state effects were present, it would be close to one. Indeed, this scaling is observed in the measurement of direct photon yield in Au+Au collisions at $\sqrt{s_{NN}} = 200$ GeV [12].

However, in Au+Au collisions at the same energy, R_{AA} for light hadrons at mid-rapidity is found to decrease from peripheral ($R_{AA} \simeq 1$) to central events ($R_{AA} \simeq 0.2$), for $p_t \gtrsim 5$ GeV (see Fig. 1). In this high- p_t region, R_{AA} is independent of the particle type and rather independent of

p_t . In Fig. 1, the data is compared to the original calculation of PQM, where the single parameter of the model was adjusted to match the suppression measured in 0–10% central Au+Au collisions at $\sqrt{s_{NN}} = 200$ GeV. For central collisions, this corresponds to an average transport coefficient of about $\langle \hat{q} \rangle = 14$ GeV²/fm, which decreases with decreasing centrality to essentially zero for the most peripheral collisions. The average is taken over all produced hard partons and given in the equivalent static scenario [11].

In Fig. 2, we show $R_{AA}(p_t)$ for neutral pions in 0–10% central Au+Au collisions at $\sqrt{s_{NN}} = 200$ GeV for preliminary PHENIX data [13], which extends beyond the previous data by almost a factor of two in p_t . The new data is compared to the original PQM calculation for $\langle \hat{q} \rangle = 14$ GeV²/fm (simply extended to larger p_t) in the reweighted and non-reweighted approximation of the quenching weights for finite (small) parton energies. For a given medium density, the reweighted values generally produce a weaker energy loss than the non-reweighted ones. However, in the reweighted case, only a rather small fraction of the full quenching weights is used. This results in the unphysical behaviour that, beyond a certain medium density, the probability of ‘zero energy loss’ increases for increasing densities. Therefore, we show in addition, results for lower densities, for $\langle \hat{q} \rangle = 4$ and 7 GeV²/fm, in the non-reweighted case. We furthermore compare the realistic calculations with calculations where we either fix the geometry ($L = 6$ fm and $\hat{q} = 1$ GeV²/fm) or the relative energy loss ($\Delta E/E = 0.25$). While the fixed geometry case leads to a more strongly rising R_{AA} with increasing p_t , the fixed relative energy loss approximation over a very wide range of p_t describes the data.

Similar conclusions can be made for the comparison with data from Cu+Cu interactions at RHIC. In Fig. 3, we show $R_{AA}(p_t)$ for neutral pions in 0–10% central Cu+Cu collisions at $\sqrt{s_{NN}} = 200$ GeV for preliminary PHENIX data [13]. The data are compared to the PQM prediction (made before QM’05 [14]) for $\langle \hat{q} \rangle = 9$ GeV²/fm for the reweighted and non-reweighted case. The value of $\langle \hat{q} \rangle = 9$ GeV²/fm relies on the proportionality of the transport coefficient to the initial volume-density of gluons [15] and on the predictions of the saturation model [16], as outlined in Ref. [10]. The prediction seems to slightly overestimate the suppression in the smaller Cu+Cu system. We therefore also present results for lower densities, for $\langle \hat{q} \rangle = 3$ and 5.5 GeV²/fm, in the non-reweighted case. As before, the calculations including the nuclear geometry are compared to calculations with either fixed geometry ($L = 4$ fm and $\hat{q} = 1$ GeV²/fm) or relative energy loss ($\Delta E/E = 0.15$).

In Fig. 4, we show calculations of the centrality dependence of the nuclear modification factor for $p_t > 7$ GeV in Cu+Cu and Au+Au collisions at $\sqrt{s_{NN}} = 200$ GeV compared to the preliminary PHENIX data [13]. The data seem to favour values for the transport coefficient of $\langle \hat{q} \rangle = 7 - 14$ for Au+Au and 3 – 5.5 GeV²/fm for Cu+Cu collisions.

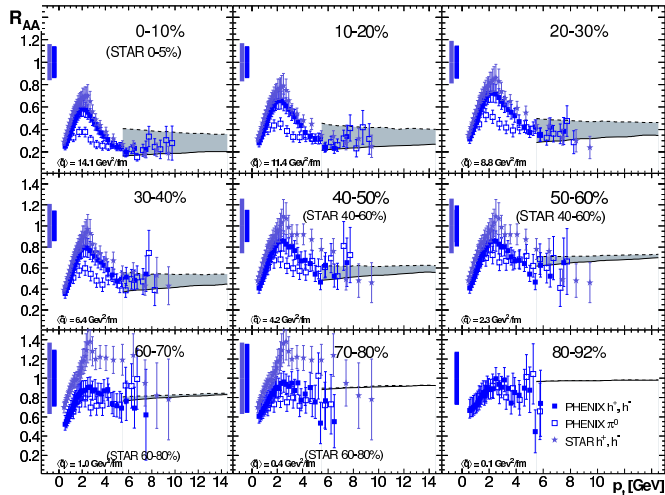


Fig. 1. $R_{AA}(p_t)$ in Au+Au at $\sqrt{s_{NN}} = 200$ GeV for different centralities. Data are PHENIX charged hadrons and π^0 [1] and STAR charged hadrons [2] with combined statistical and p_t -dependent systematic errors (bars on the data points) and p_t -independent systematic errors (bars at $R_{AA} = 1$). The gray band is the original PQM calculation from Ref. [10] using reweighted and non-reweighted quenching weights.

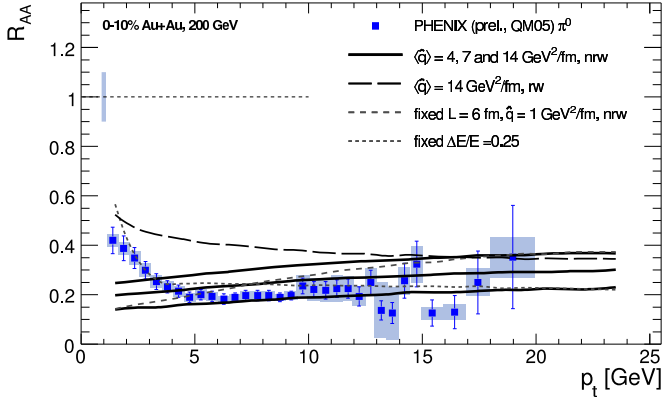


Fig. 2. $R_{AA}(p_t)$ for neutral pions in 0–10% central Au+Au collisions at $\sqrt{s_{NN}} = 200$ GeV (preliminary PHENIX data) with combined statistical and p_t -dependent systematic errors, as well as p_t -independent systematic errors (bar at $R_{AA} = 1$) [13]. The PQM curves for $\langle \hat{q} \rangle = 14$ GeV²/fm are the original PQM results (extended to larger p_t) for the reweighted and non-reweighted case from Ref. [10]. In addition, results for $\langle \hat{q} \rangle = 4$ and 7 GeV²/fm for the non-reweighted case are shown, as well as calculations for fixed $L = 6$ fm and $\hat{q} = 1$ GeV²/fm, or for fixed relative energy loss of $\Delta E/E = 0.25$.

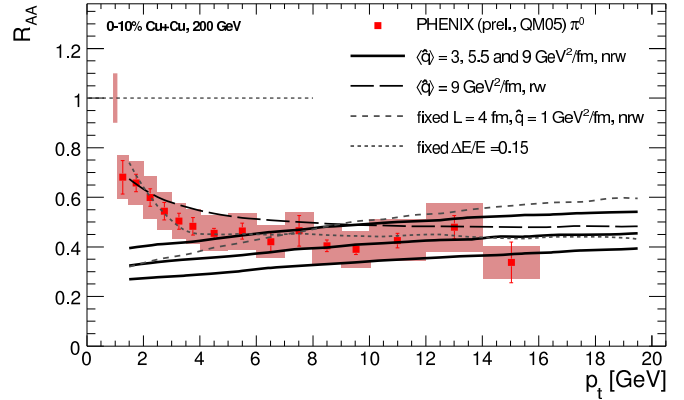


Fig. 3. $R_{AA}(p_t)$ for neutral pions in 0–10% central Cu+Cu collisions at $\sqrt{s_{NN}} = 200$ GeV (preliminary PHENIX data) with combined statistical and p_t -dependent systematic errors, as well as p_t -independent systematic errors (bar at $R_{AA} = 1$) [13]. The PQM curves for $\langle \hat{q} \rangle = 9$ GeV²/fm are the original PQM predictions for the reweighted and non-reweighted case from Ref. [10]. In addition, results for $\langle \hat{q} \rangle = 3$ and 5.5 GeV²/fm for the non-reweighted case are shown, as well as calculations for fixed $L = 4$ fm and $\hat{q} = 1$ GeV²/fm, or for fixed relative energy loss of $\Delta E/E = 0.15$.

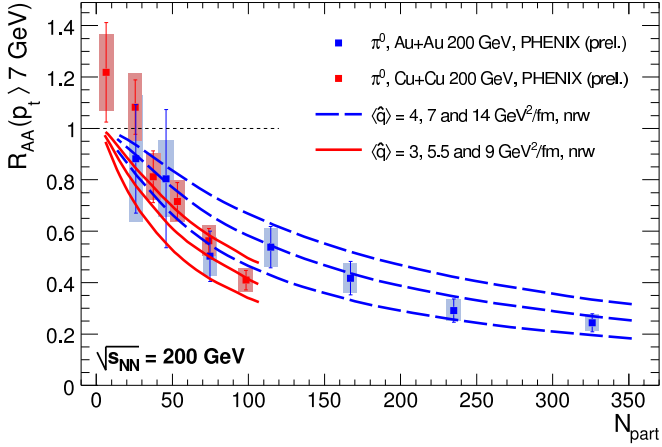


Fig. 4. Centrality dependence of $R_{AA}(p_t > 7$ GeV) for neutral pions in Cu+Cu and Au+Au collisions at $\sqrt{s_{NN}} = 200$ GeV (preliminary PHENIX data) with combined statistical and systematic errors [13]. The PQM calculation is shown for $\langle \hat{q} \rangle = 4, 7$ and 14 GeV²/fm (Au+Au), as well as for $\langle \hat{q} \rangle = 3, 5.5$ and 9 GeV²/fm (Cu+Cu) in the non-reweighted case.

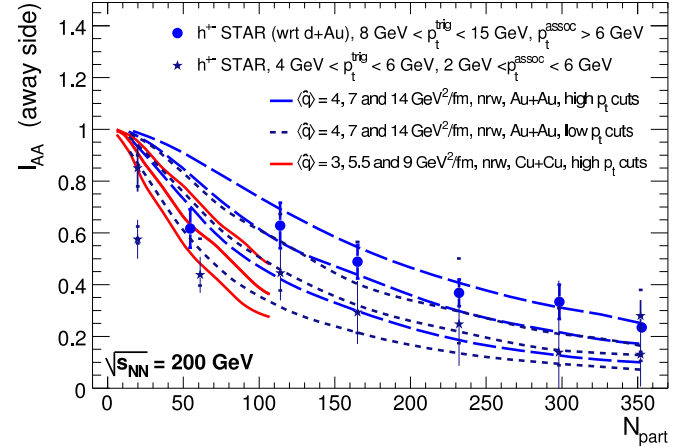


Fig. 5. Centrality dependence of I_{AA}^{away} in Au+Au at $\sqrt{s_{NN}} = 200$ GeV for two data sets. The data for the low p_t cuts of $4 < p_t^{trig} \leq 6$ GeV and 2 GeV $\leq p_t^{assoc} \leq p_t^{trig}$ with statistical (bars) and systematic (ticks) errors are from Ref. [3]. The data for the high p_t cuts of $8 < p_t^{trig} \leq 15$ GeV and 6 GeV $\leq p_t^{assoc} \leq p_t^{trig}$ with statistical (bars) errors are from Ref. [20] (wrt d+Au instead of pp). PQM results in the non-reweighted case for Au+Au are for $\langle \hat{q} \rangle = 4, 7$ and 14 GeV²/fm, and for Cu+Cu for $\langle \hat{q} \rangle = 3, 5.5$ and 9 GeV²/fm (only high trigger cuts).

4 Suppression of jet-like correlations

Within the PQM framework, we consider the suppression of back-to-back jet-like correlations by simulation of back-to-back pairs of partons in a simple LO parton model (no intrinsic k_t). The magnitude of the suppression is usually quantified by the factor $J_{AA}^{away} = D_{AA}^{away} / D_{pp}^{away}$, where the di-hadron correlation strength, $D_{pp(AA)}^{away}$, for an associated hadron, h_2 , with $p_{t,2}$ in the opposite azimuthal direction

from a trigger hadron, h_1 , with $p_{t,1}$, is integrated over the considered trigger- and associated- p_t intervals [17],

$$D_{pp(AA)}^{away} = \int_{p_{t,min}^{trig}}^{p_{t,max}^{trig}} dp_{t,1} \int_{p_{t,min}^{assoc}}^{p_{t,max}^{assoc}} dp_{t,2} \int_{away\ side} d\Delta\phi \frac{d^3\sigma_{pp(AA)}^{h_1 h_2} / dp_{t,1} dp_{t,2} d\Delta\phi}{d\sigma_{pp(AA)}^{h_1} / dp_{t,1}}, \quad (2)$$

As was found for the nuclear modification factor in Au+Au collisions at $\sqrt{s_{NN}} = 200$ GeV, I_{AA}^{away} for $4 < p_t^{trig} \leq 6$ GeV and $2 \text{ GeV} \leq p_t^{assoc} \leq p_t^{trig}$ is found to decrease with increasing centrality, down to about 0.2–0.3 for the most central events (see Fig. 5). In the figure, we also show I_{AA}^{away} data taken from Ref. [20] for higher p_t cuts of $8 < p_t^{trig} \leq 15$ GeV, where we normalize the away-side yields measured in Au+Au to the yields measured in d+Au collisions. Both data sets are compared to PQM calculations (using p+p as the reference in both cases) for the non-reweighted case with $\langle \hat{q} \rangle = 4, 7$ and $14 \text{ GeV}^2/\text{fm}$ for Au+Au collisions. The data for the higher trigger cuts favour smaller medium densities, while the uncertainties on the data for the lower cuts make it difficult to draw strong conclusions. For completeness, we also present predictions for the Cu+Cu system with $\langle \hat{q} \rangle = 3, 5.5$ and $9 \text{ GeV}^2/\text{fm}$ (only high trigger cuts).

5 Sensitivity of light hadronic probes

Another complication arises from the fact that probes based on leading-particle analyzes are affected by several biases. The biases result primarily from the steeply-falling underlying production cross sections and the emission from regions close to the surface. The latter effect dominates for large medium densities. This is illustrated in Fig. 6, which shows the behaviour of R_{AA} (at 10 GeV) and I_{AA}^{away} (for trigger cuts of $8 < p_t^{trig} \leq 15$ GeV and $6 \text{ GeV} \leq p_t^{assoc} \leq p_t^{trig}$) as a function of the medium density, expressed as $\langle \hat{q} \rangle$, in Au+Au and Cu+Cu collisions at $\sqrt{s_{NN}} = 200$ GeV. Clearly, beyond a certain medium density, the numerical values for the ratios saturate at a non-zero value. The fundamental reason is that the probability of no medium-induced gluon radiation, $P(\Delta E = 0)$, for a medium of finite size and finite density is not zero. The ‘no radiation’ contribution to the spectra is dramatically enhanced when realistic nuclear path-length distributions and density profiles are taken into account, since $P(\Delta E = 0)$ is decreasing as a function of $\hat{q} L^3$, giving significant weight to partons that ‘feel’ lower values of $\hat{q} L^3$. We have reported in Ref. [10] that the R_{AA} and I_{AA}^{away} data (for low trigger cuts) can be described by taking into account only $P(\Delta E = 0)$ and $1 - P(\Delta E = 0)$ (see also [18]).

Recently, direct measurements of dijets in heavy-ion collisions have been performed by the STAR collaboration [20]. It is found that, while the relative yields of the hadron-triggered fragmentation function relative to d+Au, the integrand in eq. (2), are suppressed, the shape is not modified, even in the most central Au+Au collisions at 200 GeV. Such a scenario naturally follows from the trigger bias since, due to the cuts on near-side and away-side particle p_t , those dijet pairs that escaped the collision region without losing a significant fraction of their initial energy are preferentially selected.

For the PQM framework, the situation is illustrated in Fig. 7, which shows production points and emission direction for surviving back-to-back pairs in the transverse plane for 0–10% central Au+Au collisions. Each parton pair shown yields a hadron pair within $8 < p_t^{trig} \leq 15$ GeV

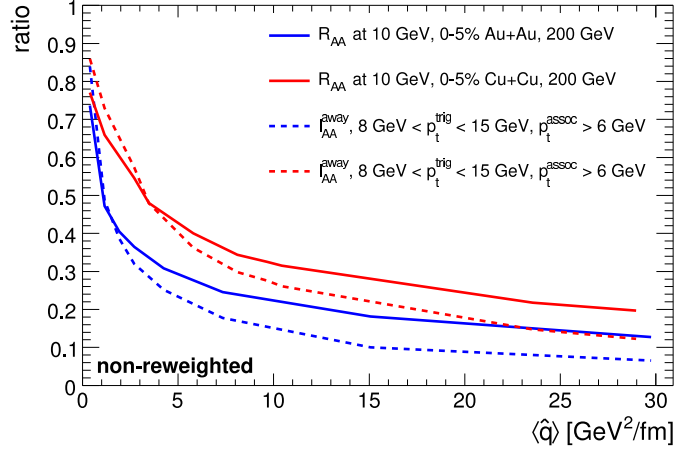


Fig. 6. R_{AA} at 10 GeV and I_{AA}^{away} for trigger cuts of $8 < p_t^{trig} \leq 15$ GeV and $6 \text{ GeV} \leq p_t^{assoc} \leq p_t^{trig}$ as a function of $\langle \hat{q} \rangle$ in 0–5% central Au+Au and Cu+Cu collisions at $\sqrt{s_{NN}} = 200$ GeV. The calculations are in the non-reweighted approximation.

and $6 \text{ GeV} \leq p_t^{assoc} \leq p_t^{trig}$. The chosen set of transport coefficients are the same as previously used to describe the I_{AA}^{away} data, $\langle \hat{q} \rangle = 4, 7$ and $14 \text{ GeV}^2/\text{fm}$, in the non-reweighted case. In panels of Fig. 7, the center of any line indicates the production point of a parton pair, and the two partons emerge along the line in opposite direction. The color of each line either indicates the medium density (left) or the relative energy loss (right panels) of the away-side parton, which is defined as the parton fragmenting into the associated hadron. The left panels of Fig. 7 clearly illustrates that the largest medium densities are encountered by away-side partons that pass through the central zone of the collision, which is expected for a static scenario. The core is surrounded by dijets that escape tangentially with respect to the central region Ref. [19]. In the case of an expanding medium, the interpretation of the underlying trigger bias remains the same: surviving dijets are always selected from regions (and times) of the collision evolution where they suffered the least amount of interactions with the medium. The right panels of Fig. 7, which color-code the relative energy loss of the away-side parton, illustrate this point from a slightly different perspective. It is apparent that in all three cases, the energy loss is close to zero for a large fraction of the dijets, even for the core region. This is due to the probability of zero-energy loss for the away-side parton, $P(\Delta E^{away} = 0)$, which for the core is already about 0.05, even for the $\langle \hat{q} \rangle = 14 \text{ GeV}^2/\text{fm}$ case. As shown in Fig. 8(a), $P(\Delta E^{away} = 0)$ quickly reaches values between 0.1 and 0.3 for the $d \lesssim 4$ fm, where $d = \sqrt{x_0^2 + y_0^2}$ is the distance of the production point to the collision center. A large fraction of these parton pairs are initially produced, see Fig. 8(b) (dashed line, no medium). The same figure illustrates the shift of the production point distribution to larger distances with increasing medium densities, when energy loss is included. The mean values change from 3.2 fm in vacuum to 3.5, 3.7 and 4.1 fm for $\langle \hat{q} \rangle = 4, 7$ and $14 \text{ GeV}^2/\text{fm}$, respectively. In Fig. 8(c), we finally present the average $\Delta E/E$ versus d for near-

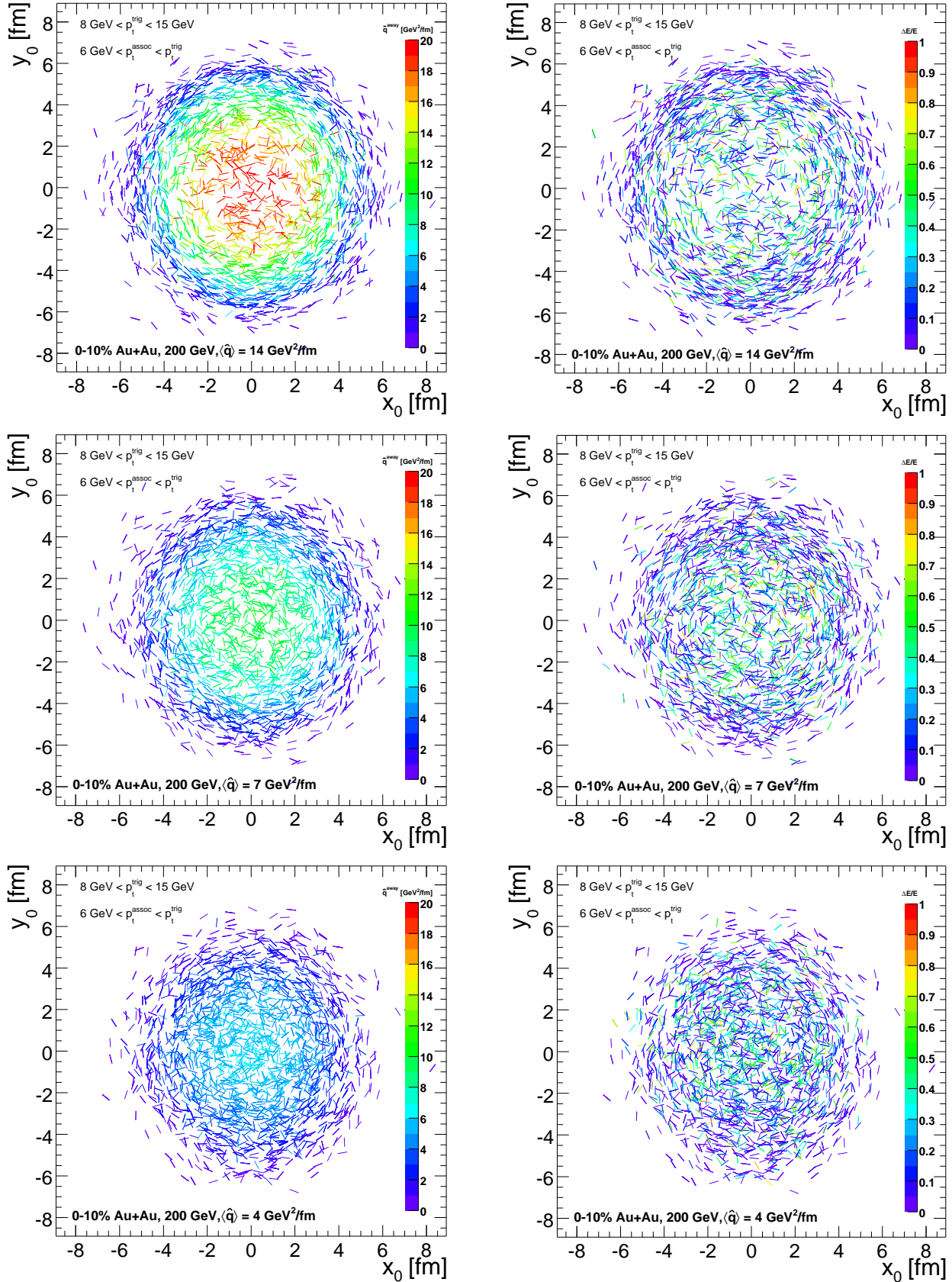


Fig. 7. (Color online) Production points and emission direction for surviving back-to-back parton pairs (yielding hadron pairs within $8 < p_t^{\text{trig}} \leq 15 \text{ GeV}$ and $6 \text{ GeV} \leq p_t^{\text{assoc}} \leq p_t^{\text{trig}}$) in the transverse plane for $\langle \hat{q} \rangle = 4$ (bottom), 7 (middle) and 14 GeV^2/fm (top panels) for 0–10% central Au+Au collisions. The line color represents the medium density (relative energy loss) of the away-side parton in the left (right) panel.

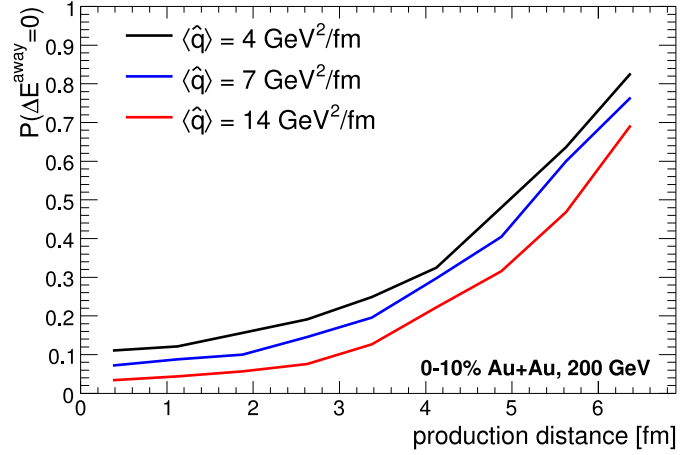
side and away-side partons. For distances of $d \gtrsim 4$ fm, that contribute significantly to the near- and away-side yields, $0.1 \lesssim \Delta E/E \lesssim 0.25$ for the three densities, and the average relative energy loss is nearly the same on both sides.

6 Summary

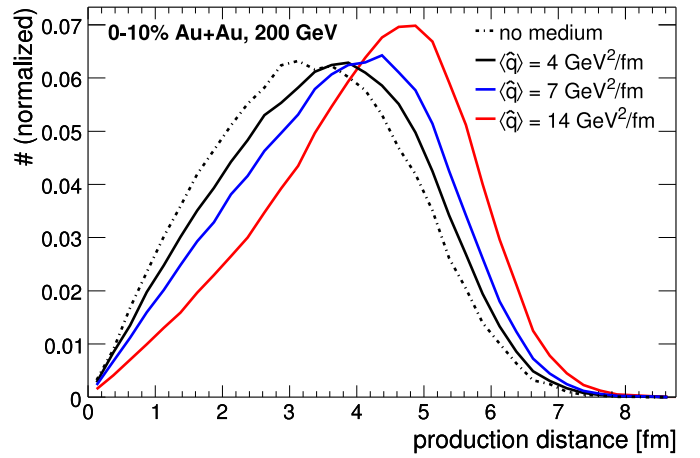
Jet quenching effects at the top RHIC energy are discussed within the Parton Quenching Model that includes a probabilistic treatment of the BDMPS quenching weights and a Glauber-based implementation of the collision geometry. The available high- p_t data for R_{AA} , I_{AA}^{away} and their centrality dependence constrain the extracted medium density to about $3 \lesssim \langle \hat{q} \rangle \lesssim 9$ GeV²/fm for central Cu+Cu and $4 \lesssim \langle \hat{q} \rangle \lesssim 14$ GeV²/fm for central Au+Au collisions. Our analysis suggests that particle production in central collisions is ‘surface’ dominated, not only for single hadrons, but also for dijets. The properties of surviving dijets therefore are very similar to the vacuum properties.

References

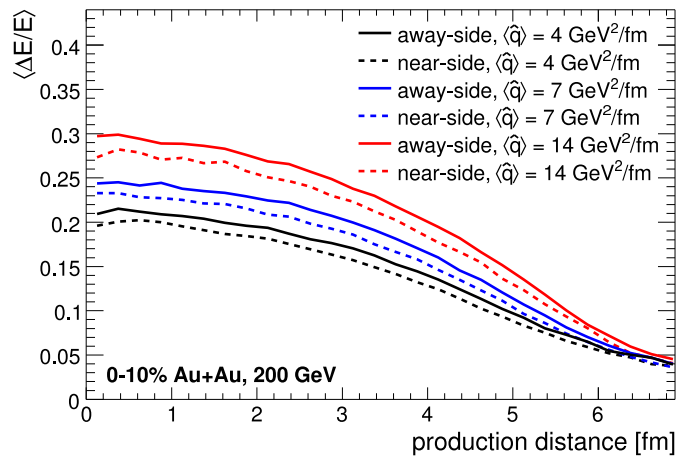
1. S.S. Adler *et al.* [PHENIX], Phys. Rev. Lett. **91** (2003) 072301, Phys. Rev. **C69** (2004) 034910.
2. J. Adams *et al.* [STAR], Phys. Rev. Lett. **91** (2003) 172302.
3. C. Adler *et al.* [STAR], Phys. Rev. Lett. **90** (2003) 082302, Phys. Rev. Lett. **95** (2005) 152301.
4. F. Antinori *et al.* [NA57], Phys. Lett. B **623** (2005) 17; C. Hohne *et al.* [NA49], nucl-ex/0510049.
5. B. Alver *et al.* [PHOBOS], Phys. Rev. Lett. **96**, 212301 (2006).
6. B.B. Back *et al.* [PHOBOS], Phys. Rev. Lett. **91** (2003) 072302; J. Adams *et al.* [STAR], *ibidem* 072304; S.S. Adler *et al.* [PHENIX], *ibidem* 072303; I. Arsene *et al.* [BRAHMS], *ibidem* 072305.
7. C.A. Salgado, hep-ph/0510062; X.N. Wang, nucl-th/0511001; I. Vitev, hep-ph/0603010.
8. A. Peshier, these proceedings, hep-ph/0607275.
9. D. d’Enterria, Eur. Phys. J. C **43**, 295 (2005).
10. A. Dainese, C. Loizides and G. Paic, Eur. Phys. J. **C38** (2005) 461.
11. C.A. Salgado and U.A. Wiedemann, Phys. Rev. **D68** (2003) 014008.
12. S. Adler *et al.* [PHENIX], Phys. Rev. Lett. **94**, 232301 (2005).
13. M. Shimomura [PHENIX], nucl-ex/0510023.
14. C. Loizides, QM’05 poster (not published), see P. M. Jacobs and M. van Leeuwen, nucl-ex/0511013.
15. R. Baier, Nucl. Phys. **A715** (2003) 209.
16. K.J. Eskola *et al.*, Nucl. Phys. **B570** (2000) 379.
17. E. Wang and X.N. Wang, Phys. Rev. Lett. **89** (2002) 162301.
18. A. Drees, H. Feng and J. Jia, Phys. Rev. C **71**, 034909 (2005).
19. A. Dainese, C. Loizides and G. Paic, hep-ph/0511045.
20. J. Adams *et al.* [STAR], nucl-ex/0604018.
21. K.J. Eskola *et al.*, Nucl. Phys. **A747** (2005) 511.



(a)



(b)



(c)

Fig. 8. (a) The probability of zero-energy loss for the away-side parton versus the distance of the production point from the collision center, (b) the distribution of production distances from the collision center and (c) the average relative energy loss for near-side and away-side partons versus the distance of the production point from the collision center for $\langle \hat{q} \rangle = 4, 7, 14$ GeV²/fm.